ARTICLES SCIENCE CHINA Materials

mater.scichina.com link.springer.com

Published online 24 September 2019 | https://doi.org/10.1007/s40843-019-1181-y

Sci China Mater 2020, 63(2): 258–266

5 nm NiCoP nanoparticles coupled with g-C_3N_4 as high-performance photocatalyst for hydrogen evolution

Bo Ma, Jinping Zhao, Zhenhua Ge, Yantao Chen* and Zhihao Yuan*

ABSTRACT **Graphitic carbon nitride (g-C_3N_4) coupled with NiCoP nanoparticles with sizes around 5 nm have been fabricated *via* a controllable alcohothermal process. NiCoP is an excellent electron conductor and cocatalyst in photocatalytic reactions. The coupling between tiny NiCoP nanoparticles and g-C_3N_4 through *in-situ* fabrication strategy could be a promising way to eliminate the light screening effect, hinder the recombination of photo-induced charge carriers, and improve the charge transfer. The NiCoP/g-C_3N_4 nanohybrids exhibit an excellent photocatalytic activity in the hydrogen generation, with a significantly improved performance compared with original g-C_3N_4, CoP/g-C_3N_4 and Ni_2P/g-C_3N_4, respectively. This study paves a new way to design transition metal phosphides-based photocatalysts for hydrogen production.**

Keywords: transition metal phosphides, photocatalytic hydrogen generation, carbon nitride, nanohybrids

INTRODUCTION

The solar power as a main source among renewable energies, has attracted a great deal of attention over the past years. Since the first report of water splitting on semiconductor-based photocatalysts by Fujishima and Honda [1] in the 1970s, photocatalysis with semiconductors has become a quite promising technique in solar energy harvesting [2]. Carbon nitride with a graphitic structure (g-C_3N_4) has great potential as non-metal and environment-friendly visible light-driven catalyst due to the tunable electronic structure [3,4]. However, due to the stacked structure, pristine g-C_3N_4 also has many drawbacks, such as low specific surface area, quick recombination of photo-induced electrons and holes, weak electrical conductivity, poor absorption of visible spectrum and utilization efficiency [5]. In order to boost the activity of g-C_3N_4, cocatalysts are introduced to avoid the rapid recombination of photo-generated charge carriers [6–12]. So far, precious metals like platinum (Pt), have been widely utilized as effective cocatalysts for photocatalytic H_2 evolution [13,14]. However, the high-cost and scarcity are the major obstacles for their practical use at a large scale. Therefore, exploring non-noble-metal cocatalysts for photocatalytic hydrogen production becomes a very important topic.

Transition metal phosphides (TMPs) have metallic characteristics and good electrical conductivity [15–19], which are desirable as cocatalysts for photocatalytic hydrogen evolution. As the important members in TMPs, the low cost and high activity of FeP [20,21], Ni_2P [22–25] and CoP [26–29] have been demonstrated as effective cocatalysts towards photocatalytic H_2 evolution. The ternary NiCoP has been reported to exhibit an enhanced electrochemical property than mono-metal phosphides on hydrogen evolution reaction (HER) [30–34]. Since it is widely accepted that an excellent HER electrocatalyst can also promote photocatalytic H_2 evolution as a co-catalyst [35,36], research on NiCoP as a competent co-catalyst has drawn considerable interests [37]. Bi *et al.* [38] adopted one-pot annealing method to fabricate a highly efficient photocatalyst of NiCoP/g-C_3N_4 with an average particle size around 10 nm for hydrogen generation. Qin *et al.* [39] synthesized a NiCoP-based core/shell cocatalyst, which was mixed with g-C_3N_4 by grinding method. Recent progress has provided evidence that the particle size is important to the catalytic activity [40,41]. Generally, reducing the particle size could improve the performance of the photocatalyst due to the enhanced quantum con-

Tianjin Key Laboratory for Photoelectric Materials and Devices, School of Materials Science and Engineering, Tianjin University of Technology, Tianjin 300384, China

* Corresponding authors (emails: chenyantao@tjut.edu.cn (Chen Y); zhyuan@tjut.edu.cn (Yuan Z))

 © Science China Press and Springer-Verlag GmbH Germany, part of Springer Nature 2019

finement effect, which will shorten the route length of photoexcited charge transmission [42–46]. In order to achieve a better photocatalytic activity, the cocatalyst, i.e., NiCoP, needs to have a tiny particle size as well as uniform distribution on the g-C_3N_4 to avoid impeding light absorption, and couple with g-C_3N_4 to improve the transfer of charge. However, the *in-situ* fabrication of g-C_3N_4 photocatalyst with uniformly distributed tiny NiCoP nanoparticles is still a challenge.

NiCoP/g-C_3N_4 nanohybrids with uniformly distributed NiCoP nanoparticles with a particle size around 5 nm are developed based on an *in-situ* growth strategy. The NiCoP/g-C_3N_4 nanohybrids possess a greatly improved photocatalytic activity than pristine g-C_3N_4 in H_2 evolution due to the enhanced charge separation and transfer, which originate from the small size of NiCoP nanoparticles, uniform distribution of NiCoP on g-C_3N_4, and the coupling between NiCoP and g-C_3N_4. The design, fabrication and in-depth characterization of NiCoP/g-C_3N_4 exhibit the great potential of TMP-based materials as noble-metal-free cocatalysts in photocatalysis for highly efficient hydrogen evolution.

EXPERIMENTAL SECTION

Chemicals

Urea, $Ni(Ac)_2{\cdot}4H_2O$, $Co(Ac)_2{\cdot}4H_2O$, 1,3-propanediol, isopropanol, sodium hypophosphite hydrate, *N*,*N*-dimethylformamide (DMF) and methanol were analytical grade and bought from Shanghai Aladdin Ltd. (China).

Synthesis of g-C_3N_4

Bulk g-C_3N_4 was fabricated by the urea precursor *via* a direct thermal condensation process. Urea powder (10 g) was placed in a 50 mL crucible with cover and then thermally treated at 550°C for 2 h under ambient atmosphere with a 5°C min^{-1} ramp rate. After naturally cooling down, the yellowish agglomerated sample was obtained and carefully ground into fine powders in an agate mortar.

Synthesis of NiCo-OH/g-C_3N_4

The NiCo hydroxides (NiCo-OH/g-C_3N_4) were fabricated by an alcohothermal method. 200 mg g-C_3N_4 was dispersed in 37.6 mL isopropanol under ultrasonication for 45 min. Meanwhile, certain amounts of $Ni(Ac)_2{\cdot}4H_2O$ (3.4, 10.2, 17, 23.8, 68 and 102 mg) and $Co(Ac)_2{\cdot}4H_2O$ (3.4, 10.2, 17, 23.8, 68 and 102 mg), corresponding to the specific loadings of NiCoP on g-C_3N_4 (1, 3, 5, 7, 20 and 30 wt%), were added into 2.4 mL of 1,3-propanediol to obtain a clear solution. The above solution was dropwise added into the g-C_3N_4 suspension. The obtained mixture was stirred for 2 h, and then moved into a Teflon-lined autoclave, maintained at 160°C for 12 h. After cooling down, the resulting product was washed by deionized water and ethanol through centrifugation, and dried at 80°C to obtain NiCo-OH/g-C_3N_4. Pristine NiCo-OH was synthesized *via* the similar steps without adding g-C_3N_4.

Synthesis of NiCoP/g-C_3N_4

The NiCoP/g-C_3N_4 was fabricated by thermal phosphidation of the as-prepared NiCo-OH/g-C_3N_4. Briefly, 0.1 g NiCo-OH/g-C_3N_4 with different loading amounts of NiCo-OH was mechanically blended with 50 mg of $NaH_2PO_2{\cdot}H_2O$ using a mortar until a uniform powder was formed. The mixture was then heated in a tube furnace with a ramp rate of 5°C min^{-1} and kept at 300°C for 2 h under Ar atmosphere. The resulting sample was washed by water and ethanol, and then dried in an oven. The final material was labeled as NiCoP-*x*/C_3N_4 (*x*=1, 3, 5, 7, 20, and 30), where *x* stands for the theoretical weight percentage of NiCoP. The same procedure was also used to obtain pristine NiCoP using 150 mg of NiCo-OH and 350 mg of $NaH_2PO_2{\cdot}H_2O$. The 3 wt% of Ni_2P and CoP on g-C_3N_4 were synthesized by the same procedure as that of NiCoP-3/C_3N_4, except for the absence of Co^{2+} or Ni^{2+} in the alcohothermal reaction, which were denoted as that of Ni_2P-3/C_3N_4 and CoP-3/C_3N_4, respectively. Thermogravimetric analysis (TGA) was conducted to confirm the actual content of cocatalysts on g-C_3N_4 (Fig. S1). TGA results show that the actual weight percentage of NiCoP, N_2P and CoP on g-C_3N_4 is very close to the theoretical value.

Characterization

The X-ray diffraction (XRD) was obtained from a Rigaku SmartLab using Cu Kα radiation. X-ray photoelectron spectra (XPS) and ultraviolet photoelectron spectra (UPS) were measured on a Thermo Fisher Scientific ESCALAB 250Xi. Scanning electron microscopy (SEM) imaging was conducted on a FEI Verios 460L. Transmission electron microscopy (TEM) imaging, high resolution TEM (HRTEM) imaging and scanning TEM (STEM) imaging were implemented on a JEOL JEM-3010. UV-Vis diffuse reflectance spectra were examined by a PerkinElmer Lambda 750 with $BaSO_4$ standard. Photoluminescence (PL) spectrum was recorded at ambient temperature on a Hitachi F-4600 fluorescence spectrophotometer with 365 nm excitation wavelength. TGA was performed under 30% O_2/N_2 at a heating rate of 10 K min^{-1} on a TA

 © Science China Press and Springer-Verlag GmbH Germany, part of Springer Nature 2019

SDT Q600 analyzer.

Photocatalytic evaluations

The photocatalytic activities for hydrogen generation were assessed in a gastight and evacuation system connected circulation, in which a top-irradiation-type Pyrex cell and a 300 W xenon lamp with 300–780 nm wavelength were used. 100 mg photocatalyst was dispersed in the reactor containing 10 mL methanol and 90 mL water under vigorous stirring. The suspension was degassed by evacuation for 15 min before irradiation. The temperature of the reactor was kept at 20°C by a flowing circular water-cooling system. The amount of evolved hydrogen was analyzed by an on-line gas chromatograph (Techcomp GC7900, TCD detector and 5A molecular sieve capillary column, Ar as carrier gas). The apparent quantum efficiency (AQE) was measured under the same condition as that of photocatalytic reaction, except using a 420 nm band pass filter. The intensity of monochromatic light on the reactor was ~6.2 mW cm^{-2} over an area of 19.6 cm^2. The AQE was calculated using the following Equation (1):

$$\mathrm{AQE}(\%) = \frac{\text{number of reacted electrons}}{\text{number of incident photons}} \times 100 = \frac{\text{number of evolved } H_2 \text{ molecules} \times 2}{\text{number of incident photons}} \times 100. \quad (1)$$

Electrochemical analysis

The electrochemical properties were tested on a Chenhua CHI 760E electrochemical workstation by employing a standard three-electrode cell in 0.5 mol L^{-1} Na_2SO_4 solution. The light source was a 300 W Xe lamp equipped with a 400 nm cutoff filter. The reference electrode and counter electrode were Ag/AgCl (saturated KCl) and Pt foil (1×2 cm^2), respectively. The working electrode for electrochemical measurements was prepared as follow: 1 mg sample was ultrasonically dispersed in DMF and then milled to form homogeneous paste. The paste was uniformly deposited over indium tin oxide (ITO) glass with 2.0 cm^2 of exposed area, and annealed at 300°C under Ar atmosphere.

RESULTS AND DISCUSSION

Fig. 1 displays the XRD results of original g-C_3N_4 and different NiCoP-x/C_3N_4 (x = 1, 3, 5, 7, 20 and 30). All the samples have two characteristic diffraction peaks at 13.0° and 27.4° indexed to g-C_3N_4, which are attributed to the (100) plane with in-plane repeating period of heptazine framework and the (002) plane with interlayer stacking of conjugated aromatic structures [47,48]. For the NiCoP-x/C_3N_4, when the content of NiCoP is below 20%, the diffraction peaks corresponding to NiCoP cannot be observed due to the small amount and the high dispersity. As the content of NiCoP increases to 20%, obvious diffraction peaks of NiCoP are observed. The diffraction peaks located at 41° and 44.9° could be indexed to (111) and (201) planes of hexagonal NiCoP (JCPDS No. 71-2336), respectively.

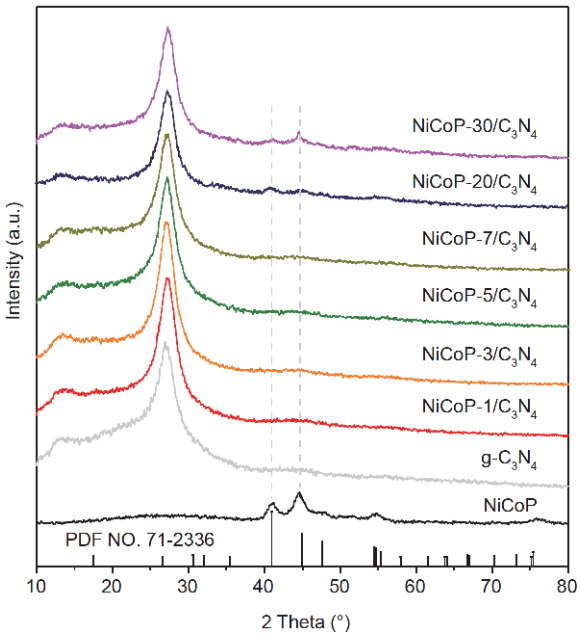

Figure 1 XRD results of NiCoP, g-C_3N_4 and NiCoP-x/C_3N_4.

The surface chemical composition of the as-fabricated NiCoP-3/C_3N_4 was probed by XPS. The XPS survey spectrum (Fig. 2a) confirms the existence of Ni, Co, and P. In the C 1s region (Fig. 2b), the peaks located at 284.7, 288.2 and 285.8 eV correspond to the C–C, N–C=N, and C–NH_2 in g-C_3N_4 [49,50]. The N 1s region of g-C_3N_4 (Fig. 2c) is deconvoluted into four peaks at 398.6, 399.4, 400.8 and 404.7 eV, attributed to the C–N=C, N–$(C)_3$, C–N–H and π-excitations of the C=N conjugated systems from g-C_3N_4, respectively [51,52]. The two peaks of the Ni 2p region (Fig. 2d) located at 853.3 eV (Ni $2p_{3/2}$) and 868.5 eV (Ni $2p_{1/2}$) imply the presence of partially charged $Ni^{\delta+}$ ($\delta \approx 0$) in Ni-P compound, and the peaks around 856.4 and 872.7 eV can be ascribed to oxidized Ni^{2+}. The peaks at 862.1 eV (Ni $2p_{3/2}$) and 880.0 eV (Ni $2p_{1/2}$) are assigned to the satellites [53,54]. In Co 2p region (Fig. 2e), the peak at 778.5 eV is ascribed to Co $2p_{3/2}$ of partially charged reduced $Co^{\delta+}$ ($\delta \approx 0$) in the

© Science China Press and Springer-Verlag GmbH Germany, part of Springer Nature 2019

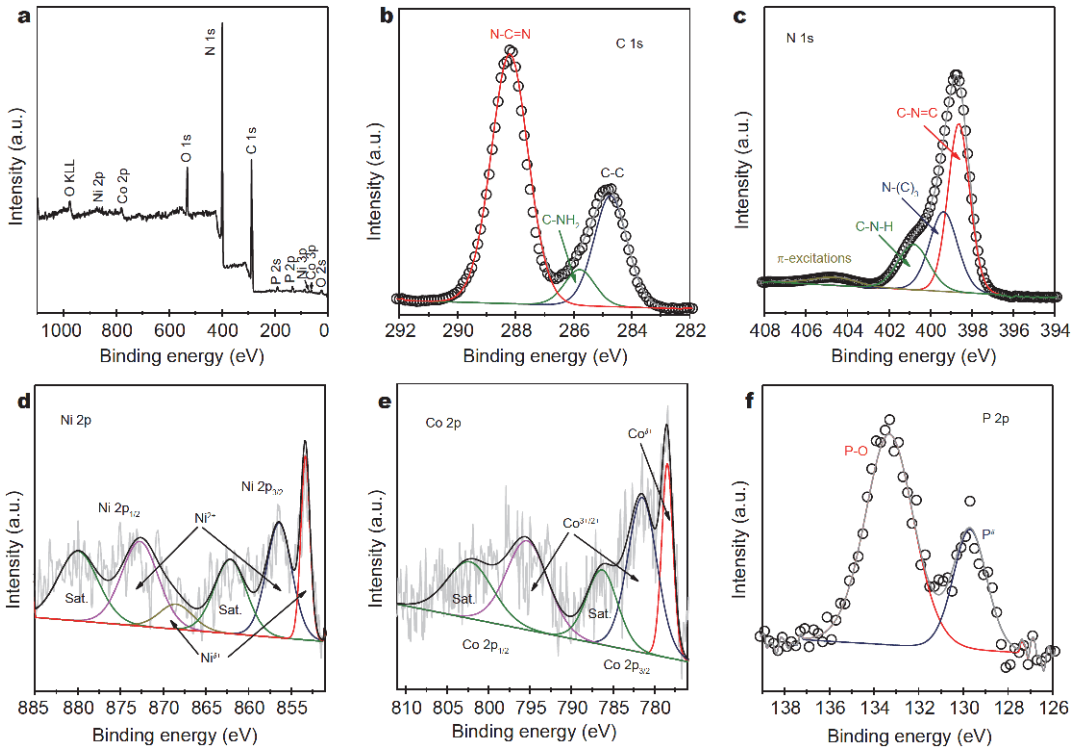

Figure 2 XPS survey spectrum (a) and C 1s (b), N 1s (c), Ni 2p (d), Co 2p (e) and P 2p (f) spectra of NiCoP-3/C_3N_4.

Co-P compound. Besides, the peaks at 781.5 and 795.4 eV are attributed to Co $2p_{3/2}$ and Co $2p_{1/2}$ of the oxidized $Co^{2+/3+}$, with satellite peaks at 786.3 and 802.3 eV [55,56]. In the P 2p spectrum (Fig. 2f), the peak at 129.7 eV can be ascribed to the reduced $P^{\delta-}$ in the metal phosphides, while the peak at 133.3 eV can be assigned to the phosphorus oxide (denoted as P^{5+}) due to the exposure to air [57]. Since the XPS signals of Ni 2p and Co 2p in NiCoP-3/C_3N_4 are weak for the low content of NiCoP, the XPS of pristine NiCoP shown in Fig. S2 displays almost the same deconvolution peaks as NiCoP-3/C_3N_4.

The SEM image of NiCoP-3/C_3N_4 is shown in Fig. 3a. The as-prepared NiCoP-3/C_3N_4 aggregates as a highly crumpled structure. The corresponding energy dispersive X-ray spectrometry (EDX) elemental mapping suggests that Ni, Co, and P are evenly spread over the surface of NiCoP-3/C_3N_4 (Fig. S3). The structure and composition of NiCoP-3/C_3N_4 were further characterized by TEM. The TEM image reveals that the bare g-C_3N_4 is composed of irregularly curved layers (Fig. S4). For NiCoP-3/C_3N_4, the tiny nanoparticles are evenly distributed on the g-C_3N_4 nanosheets (Fig. 3b, c). In the synthesis process, the metal ions (Ni^{2+} and $Co^{2+/3+}$) can be captured by the lone pair electrons of nitrogen in the g-C_3N_4 framework, leading to a uniform distribution [5]. The average particle size of the NiCoP nanoparticles was calculated as 5 nm (Fig. S5). The HRTEM image (Fig. 3d) of the single NiCoP nanoparticle on g-C_3N_4 clearly presents the (111) plane of NiCoP, with lattice spacing of 0.22 nm [58]. The STEM image and elemental mapping of nanohybrids are demonstrated in Fig. 3e, revealing Ni, Co and P elements are concentrated on NiCoP nanoparticles. The TEM EDX spectrum is given in Fig. S6, suggesting the atomic ratio of Ni:Co:P is around 5:4:5.

The UV-Vis absorption analysis was used to investigate the optical property of g-C_3N_4, NiCoP and NiCoP-x/C_3N_4 (Fig. 4a). The colors of the as-prepared NiCoP-x/C_3N_4 samples vary from yellow to dark gray (Fig. S7). Besides, NiCoP-x/C_3N_4 exhibits remarkably raised absorption in the whole visible spectrum range with increased content of NiCoP, which should be attributed to the inherent absorption of NiCoP nanoparticles. The band gaps of original g-C_3N_4 and NiCoP-3/C_3N_4 calculated from the derived plots of the transformed Kubelka–Munk functions are 2.68 and 2.62 eV, respectively. The almost same value indicates that loading of NiCoP does not cause any obvious change of the intrinsic band gap of the original g-C_3N_4 (Fig. 4b).

In order to further study the band edge positions of NiCoP-3/C_3N_4, Mott–Schottky measurements were car-

 © Science China Press and Springer-Verlag GmbH Germany, part of Springer Nature 2019

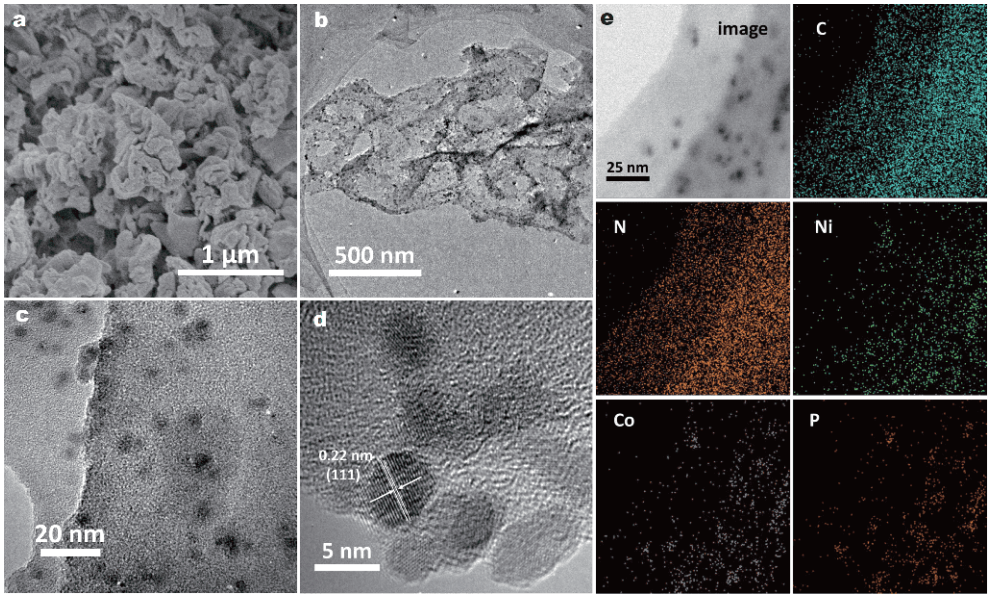

Figure 3 (a) SEM, (b, c) TEM, (d) HRTEM images and (e) STEM elemental mapping of NiCoP-3/C_3N_4.

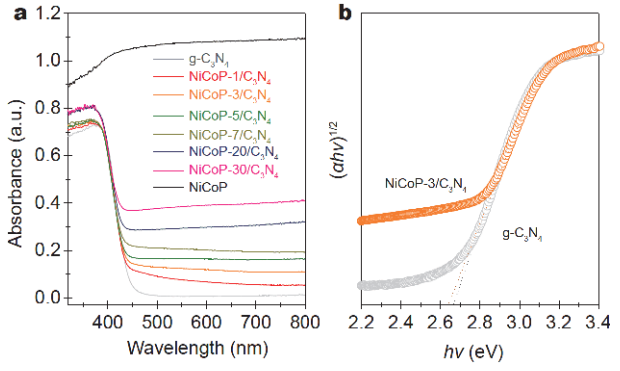

Figure 4 (a) UV-Vis absorption spectrum and (b) the corresponding plots of $(\alpha h\nu)^{1/2}$ *versus* $h\nu$ of g-C_3N_4 and NiCoP-x/C_3N_4 samples.

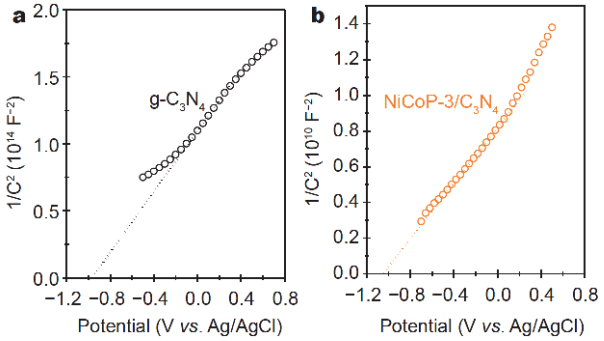

Figure 5 Mott–Schottky plots of g-C_3N_4 and NiCoP-3/C_3N_4.

ried out as displayed in Fig. 5. The Mott–Schottky plots of g-C_3N_4 and NiCoP-3/C_3N_4 show positive slopes, corresponding to n-type semiconductors. The flat-band potentials of g-C_3N_4 and NiCoP-3/C_3N_4 can be estimated as −0.76 and −0.84 V *vs.* the normal hydrogen electrode (NHE, $E_{NHE}=E_{Ag/AgCl}+0.197$ V) [59], which are obtained from the *x*-axis intercept of the linear region in Mott–Schottky plots. Normally, the flat band potential of n-type semiconductor is more positive about 0.1 or 0.2 V than its conduction band potential [60], so the calculated conduction band bottoms of g-C_3N_4 and NiCoP-3/C_3N_4 from Mott-Schottky plots are determined as −0.96 and −1.04 V *vs.* NHE, respectively. According to the equation $E_{VB} = E_{CB} + E_g$ [61], the E_{VB} of g-C_3N_4 and NiCoP-3/C_3N_4 are calculated as 1.72 and 1.58 V, *vs.* NHE, respectively. For comparison, UPS was also employed to measure the valence band of g-C_3N_4 and NiCoP-3/C_3N_4, as given in Fig. S8. The valence band tops of g-C_3N_4 and NiCoP-3/C_3N_4 are determined as 1.84 and 1.68 V, respectively *vs.* NHE, which are close to the results of Mott–Schottky plots. Obviously, coupling with tiny NiCoP nanoparticles leads to a variation in the band structure of g-C_3N_4. Considering band edge positions of the as-prepared NiCoP-3/C_3N_4, it should be a promising photocatalyst under UV-Vis light.

The light harvesting properties of NiCoP-x/C_3N_4 were investigated for photocatalytic H_2 generation. As shown in Fig. 6, only a trace amount of H_2 could be detected for pristine g-C_3N_4, while NiCoP exhibits no appreciable activity under UV-Vis light irradiation. However, NiCoP

 © Science China Press and Springer-Verlag GmbH Germany, part of Springer Nature 2019

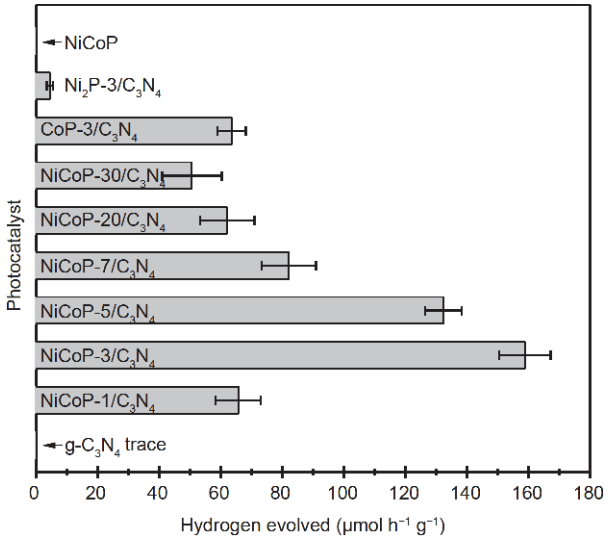

Figure 6 Photocatalytic H_2 generation activities of different samples under UV-Vis light. 100 mg photocatalyst and 10 mL methanol in 90 mL water, T = 298 K.

can significantly promote the photocatalytic hydrogen evolution when coupling with g-C_3N_4. The enhancement effect of NiCoP is strongly related to its weight percentage and a volcano-shaped curve can be plotted. The highest photocatalytic H_2 generation rate of 159 μmol g^{-1} h^{-1} is obtained for NiCoP-3/C_3N_4, which is increased by a factor of 2.5 folds compared with CoP-3/C_3N_4 and 35 folds compared with Ni_2P-3/C_3N_4. The AQE is calculated as 4.2% for the optimized NiCoP-3/C_3N_4 photocatalyst under monochromatic 420 nm visible light, which is one of the highest values among the similar TMPs/g-C_3N_4 photocatalytic systems (Table S1). The activity of NiCoP-3/C_3N_4 was compared with the 3 wt% Pt loaded g-C_3N_4 (Pt-3/C_3N_4) (Fig. S9). Although Pt-3/C_3N_4 has a higher photocatalytic activity, NiCoP-3/C_3N_4 has the obvious advantage of low-cost. In addition, the photo-stability of NiCoP-3/C_3N_4 was also evaluated by performing cycling tests. As indicated in Fig. S10, after five cycling tests, the activity had no obvious loss, confirming the sufficient stability of NiCoP-3/C_3N_4 for photocatalytic H_2 evolution.

Under suitable light irradiation, the electrons of g-C_3N_4 are excited from valence band (VB) into conduction band (CB), and holes are left in the VB. The photo-generated charges can migrate to the solid–solution interface of g-C_3N_4, reducing water to hydrogen and oxidizing methanol. However, a rapid recombination of the charges occurs in bare g-C_3N_4 with the absence of cocatalysts. NiCoP is identified as an excellent electron conductor. When coupling with g-C_3N_4, photo-induced electrons in the CB of g-C_3N_4 will efficiently move to the surface of NiCoP, and react with water to generate hydrogen. At the same time, the holes in the VB of g-C_3N_4 are consumed for oxidizing methanol. The NiCoP nanoparticles can effectively restrain the recombination of photo-induced electron-hole pairs, and thereby facilitate the photocatalytic activity. With the increasing content of NiCoP, the transfer of photo-induced electrons in NiCoP-x/C_3N_4 should be promoted, whereas the light absorbance would be diminished by the light screening effect, and the agglomeration of excess NiCoP also decreases the activity of reaction sites. To balance these two points, NiCoP-3/C_3N_4 was optimized for effective hydrogen evolution (Fig. 7).

PL spectrum is very helpful to explore the electron-hole pairs separation and migration behaviors in semiconductor materials. The emission PL spectra of g-C_3N_4 and NiCoP-x/C_3N_4 were measured at room temperature and shown in Fig. 8. PL signals of all samples are located within 400–600 nm as a result of the surface and internal radiative recombination of photo-induced charges. It is observed that the presence of NiCoP significantly decreases the PL intensity, confirming the role of NiCoP in boosting the charge transfer and suppressing the charge recombination in g-C_3N_4. The high separation efficiency leads to a higher performance of NiCoP-x/C_3N_4. Compared with Ni_2P and CoP cocatalysts, the lower PL intensity indicates NiCoP is more efficient to suppress the charge recombination (Fig. S11).

To reveal the charge-transfer behavior in g-C_3N_4 and NiCoP-3/C_3N_4 photocatalysts, photocurrent responses were finally examined, as shown in Fig. 9a. Pristine g-C_3N_4 shows an obvious current response from potential

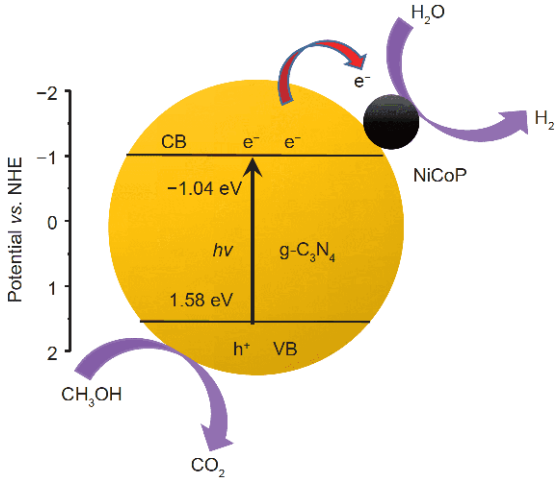

Figure 7 Schematic of the separation of photo-generated charge carriers in the photocatalytic H_2 generation for the NiCoP/g-C_3N_4 nanohybrids.

 © Science China Press and Springer-Verlag GmbH Germany, part of Springer Nature 2019

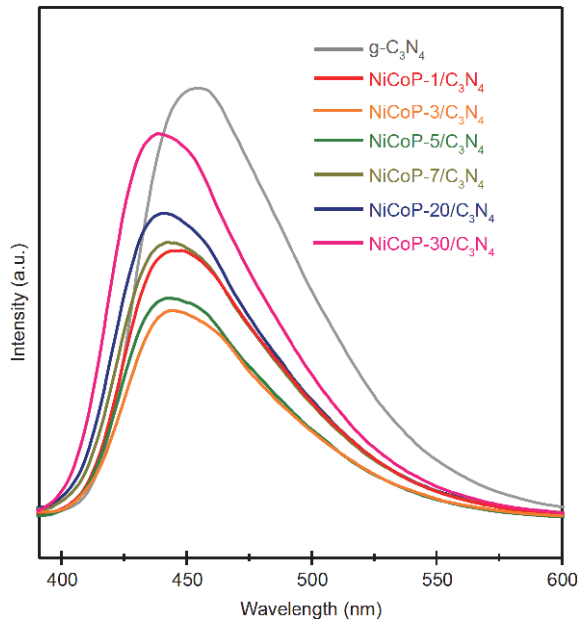

Figure 8 PL spectra of g-C_3N_4 and NiCoP-x/C_3N_4.

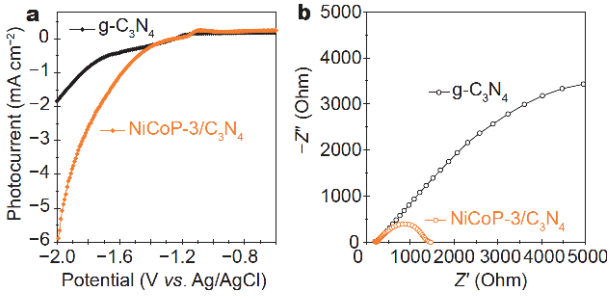

Figure 9 (a) Photocurrent responses and (b) EIS result of g-C_3N_4 and NiCoP-3/C_3N_4 under ≥400 nm light.

of −1.1 V (*vs.* Ag/AgCl) under light with wavelength ≥400 nm. NiCoP-3/C_3N_4 shows a much higher photocurrent density, suggesting the presence of NiCoP significantly enhances the separation and migration efficiency of photo-induced charge carriers. Fig. 9b displays the electrochemical impedance spectroscopy (EIS) of the as-fabricated pristine g-C_3N_4 and NiCoP-3/C_3N_4. The diameter of the semicircle in the Nyquist plots is relative to the charge transfer resistance (R_{ct}). The value of R_{ct} concluded from the EIS of NiCoP-3/C_3N_4 is much smaller than that of pristine g-C_3N_4, reflecting the more rapid electron transfer in NiCoP-3/C_3N_4 photocatalyst. The R_{ct} value of NiCoP-3/C_3N_4 is also much smaller than that of Ni_2P-3/C_3N_4 and CoP-3/C_3N_4 (Fig. S12), supporting the conclusion that NiCoP has a better charge transfer efficiency than Ni_2P and CoP.

CONCLUSIONS

The NiCoP/g-C_3N_4 nanohybrids containing uniformly distributed 5 nm NiCoP nanoparticles coupled with g-C_3N_4 nanosheets were successfully developed *via* an *in-situ* growth strategy. Considering NiCoP as an excellent electron conductor, the photo-induced electrons in g-C_3N_4 may efficiently move to NiCoP, and the recombination of photo-induced charges should be largely suppressed. Accordingly, NiCoP/g-C_3N_4 nanohybrids exhibit greatly enhanced photocatalytic activity than pristine g-C_3N_4. The enhancement effects of NiCoP cocatalyst are relative with NiCoP contents and the optimized NiCoP weight percentage is 3 wt%, leading to a hydrogen production rate of 159 μmol g^{-1} h^{-1} by using UV-Vis light, which is significantly higher than pristine g-C_3N_4, CoP/C_3N_4 and Ni_2P/C_3N_4, respectively. The *in-situ* fabrication of tiny NiCoP nanoparticles coupled with g-C_3N_4 as a highly active photocatalyst in hydrogen production demonstrates an effective strategy for boosting the photocatalytic activity of noble-metal-free cocatalyst.

Received 24 June 2019; accepted 5 September 2019; published online 24 September 2019

1 Fujishima A, Honda K. Electrochemical photolysis of water at a semiconductor electrode. Nature, 1972, 238: 37–38
2 Ravelli D, Dondi D, Fagnoni M, *et al.* Photocatalysis. A multifaceted concept for green chemistry. Chem Soc Rev, 2009, 38: 1999
3 Thomas A, Fischer A, Goettmann F, *et al.* Graphitic carbon nitride materials: Variation of structure and morphology and their use as metal-free catalysts. J Mater Chem, 2008, 18: 4893–4908
4 Wang Y, Wang X, Antonietti M. Polymeric graphitic carbon nitride as a heterogeneous organocatalyst: From photochemistry to multipurpose catalysis to sustainable chemistry. Angew Chem Int Ed, 2012, 51: 68–89
5 Ong WJ, Tan LL, Ng YH, *et al.* Graphitic carbon nitride (g-C_3N_4)-based photocatalysts for artificial photosynthesis and environmental remediation: Are we a step closer to achieving sustainability? Chem Rev, 2016, 116: 7159–7329
6 Liu J, Liu Y, Liu N, *et al.* Metal-free efficient photocatalyst for stable visible water splitting *via* a two-electron pathway. Science, 2015, 347: 970–974
7 Han C, Li J, Ma Z, *et al.* Black phosphorus quantum dot/g-C_3N_4 composites for enhanced CO_2 photoreduction to CO. Sci China Mater, 2018, 61: 1159–1166
8 Cheng F, Yin H, Xiang Q. Low-temperature solid-state preparation of ternary CdS/g-C_3N_4/CuS nanocomposites for enhanced visible-light photocatalytic H_2-production activity. Appl Surf Sci, 2017, 391: 432–439
9 Dong J, Shi Y, Huang C, *et al.* A new and stable Mo-Mo_2C modified g-C_3N_4 photocatalyst for efficient visible light photocatalytic H_2 production. Appl Catal B-Environ, 2019, 243: 27–35
10 Kong L, Dong Y, Jiang P, *et al.* Light-assisted rapid preparation of a Ni/g-C_3N_4 magnetic composite for robust photocatalytic H_2 evolution from water. J Mater Chem A, 2016, 4: 9998–10007
11 Qin Z, Wang M, Li R, *et al.* Novel Cu_3P/g-C_3N_4 p-n heterojunction

 © Science China Press and Springer-Verlag GmbH Germany, part of Springer Nature 2019

photocatalysts for solar hydrogen generation. Sci China Mater, 2018, 61: 861–868
12 Hu C, Han Q, Zhao F, *et al.* Graphitic C_3N_4-Pt nanohybrids supported on a graphene network for highly efficient methanol oxidation. Sci China Mater, 2015, 58: 21–27
13 Martin DJ, Qiu K, Shevlin SA, *et al.* Highly efficient photocatalytic H_2 evolution from water using visible light and structure-controlled graphitic carbon nitride. Angew Chem Int Ed, 2014, 53: 9240–9245
14 Tang Y, Zhou P, Chao Y, *et al.* Face-to-face engineering of ultrathin Pd nanosheets on amorphous carbon nitride for efficient photocatalytic hydrogen production. Sci China Mater, 2019, 62: 351–358
15 Tian L, Yan X, Chen X. Electrochemical activity of iron phosphide nanoparticles in hydrogen evolution reaction. ACS Catal, 2016, 6: 5441–5448
16 Song J, Xiang J, Mu C, *et al.* Facile synthesis and excellent electrochemical performance of CoP nanowire on carbon cloth as bifunctional electrode for hydrogen evolution reaction and supercapacitor. Sci China Mater, 2017, 60: 1179–1186
17 Wang X, Li W, Xiong D, *et al.* Bifunctional nickel phosphide nanocatalysts supported on carbon fiber paper for highly efficient and stable overall water splitting. Adv Funct Mater, 2016, 26: 4067–4077
18 Tian J, Liu Q, Cheng N, *et al.* Self-supported Cu_3P nanowire arrays as an integrated high-performance three-dimensional cathode for generating hydrogen from water. Angew Chem Int Ed, 2014, 53: 9577–9581
19 Zhang J, Sui R, Xue Y, *et al.* Direct synthesis of parallel doped N-MoP/N-CNT as highly active hydrogen evolution reaction catalyst. Sci China Mater, 2019, 62: 690–698
20 Zhao H, Wang J, Dong Y, *et al.* Noble-metal-free iron phosphide cocatalyst loaded graphitic carbon nitride as an efficient and robust photocatalyst for hydrogen evolution under visible light irradiation. ACS Sustain Chem Eng, 2017, 5: 8053–8060
21 Xu J, Qi Y, Wang C, *et al.* NH_2-MIL-101(Fe)/Ni(OH)$_2$-derived C, N-codoped Fe_2P/Ni_2P cocatalyst modified g-C_3N_4 for enhanced photocatalytic hydrogen evolution from water splitting. Appl Catal B-Environ, 2019, 241: 178–186
22 Wang W, An T, Li G, *et al.* Earth-abundant Ni_2P/g-C_3N_4 lamellar nanohydrids for enhanced photocatalytic hydrogen evolution and bacterial inactivation under visible light irradiation. Appl Catal B-Environ, 2017, 217: 570–580
23 Zeng D, Xu W, Ong WJ, *et al.* Toward noble-metal-free visible-light-driven photocatalytic hydrogen evolution: Monodisperse sub–15 nm Ni_2P nanoparticles anchored on porous g-C_3N_4 nanosheets to engineer 0D-2D heterojunction interfaces. Appl Catal B-Environ, 2018, 221: 47–55
24 Sun Z, Zheng H, Li J, *et al.* Extraordinarily efficient photocatalytic hydrogen evolution in water using semiconductor nanorods integrated with crystalline Ni_2P cocatalysts. Energy Environ Sci, 2015, 8: 2668–2676
25 Xu J, Qi Y, Wang L. *In situ* derived Ni_2P/Ni encapsulated in carbon/g-C_3N_4 hybrids from metal–organic frameworks/g-C_3N_4 for efficient photocatalytic hydrogen evolution. Appl Catal B-Environ, 2019, 246: 72–81
26 Pan Z, Zheng Y, Guo F, *et al.* Decorating CoP and Pt nanoparticles on graphitic carbon nitride nanosheets to promote overall water splitting by conjugated polymers. ChemSusChem, 2017, 10: 87–90
27 Zhao H, Jiang P, Cai W. Graphitic C_3N_4 decorated with CoP co-catalyst: Enhanced and stable photocatalytic H_2 evolution activity from water under visible-light irradiation. Chem Asian J, 2017, 12: 361–365
28 Dong Y, Kong L, Wang G, *et al.* Photochemical synthesis of Co_xP as cocatalyst for boosting photocatalytic H_2 production *via* spatial charge separation. Appl Catal B-Environ, 2017, 211: 245–251
29 Wang XJ, Tian X, Sun YJ, *et al.* Enhanced Schottky effect of a 2D–2D CoP/g-C_3N_4 interface for boosting photocatalytic H_2 evolution. Nanoscale, 2018, 10: 12315–12321
30 Ma B, Yang Z, Chen Y, *et al.* Nickel cobalt phosphide with three-dimensional nanostructure as a highly efficient electrocatalyst for hydrogen evolution reaction in both acidic and alkaline electrolytes. Nano Res, 2019, 12: 375–380
31 Hu E, Feng Y, Nai J, *et al.* Construction of hierarchical Ni–Co–P hollow nanobricks with oriented nanosheets for efficient overall water splitting. Energy Environ Sci, 2018, 11: 872–880
32 Zhang R, Wang X, Yu S, *et al.* Ternary $NiCo_2P_x$ nanowires as pH-universal electrocatalysts for highly efficient hydrogen evolution reaction. Adv Mater, 2017, 29: 1605502
33 Liang H, Gandi AN, Anjum DH, *et al.* Plasma-assisted synthesis of NiCoP for efficient overall water splitting. Nano Lett, 2016, 16: 7718–7725
34 Du C, Yang L, Yang F, *et al.* Nest-like NiCoP for highly efficient overall water splitting. ACS Catal, 2017, 7: 4131–4137
35 Qin Z, Chen Y, Huang Z, *et al.* Composition-dependent catalytic activities of noble-metal-free NiS/Ni_3S_4 for hydrogen evolution reaction. J Phys Chem C, 2016, 120: 14581–14589
36 Zhao H, Sun S, Jiang P, *et al.* Graphitic C_3N_4 modified by Ni_2P cocatalyst: An efficient, robust and low cost photocatalyst for visible-light-driven H_2 evolution from water. Chem Eng J, 2017, 315: 296–303
37 Xu J, Qi Y, Wang W, *et al.* Montmorillonite-hybridized g-C_3N_4 composite modified by NiCoP cocatalyst for efficient visible-light-driven photocatalytic hydrogen evolution by dye-sensitization. Int J Hydrogen Energy, 2019, 44: 4114–4122
38 Bi L, Gao X, Zhang L, *et al.* Enhanced photocatalytic hydrogen evolution of NiCoP/g-C_3N_4 with improved separation efficiency and charge transfer efficiency. ChemSusChem, 2018, 11: 276–284
39 Qin Z, Chen Y, Huang Z, *et al.* A bifunctional NiCoP-based core/shell cocatalyst to promote separate photocatalytic hydrogen and oxygen generation over graphitic carbon nitride. J Mater Chem A, 2017, 5: 19025–19035
40 Henderson MA. A surface science perspective on TiO_2 photocatalysis. Surf Sci Rep, 2011, 66: 185–297
41 Wang D, Liu ZP, Yang WM. Revealing the size effect of platinum cocatalyst for photocatalytic hydrogen evolution on TiO_2 support: A DFT study. ACS Catal, 2018, 8: 7270–7278
42 Jiu J, Wang F, Adachi M. Preparation of highly photocatalytic active nano-scale TiO_2 by mixed template method. Mater Lett, 2004, 58: 3915–3919
43 Yeung KL, Maira AJ, Stolz J, *et al.* Ensemble effects in nanostructured TiO_2 used in the gas-phase photooxidation of trichloroethylene. J Phys Chem B, 2002, 106: 4608–4616
44 Shtein M, Nadiv R, Buzaglo M, *et al.* Thermally conductive graphene-polymer composites: Size, percolation, and synergy effects. Chem Mater, 2015, 27: 2100–2106
45 Meng Q, Zhou Y, Chen G, *et al.* Integrating both homojunction and heterojunction in QDs self-decorated Bi_2MoO_6/BCN composites to achieve an efficient photocatalyst for Cr(VI) reduction. Chem Eng J, 2018, 334: 334–343

 © Science China Press and Springer-Verlag GmbH Germany, part of Springer Nature 2019

46 Lu Z, Li C, Han J, *et al.* Construction 0D/2D heterojunction by highly dispersed Ni_2P QDs loaded on the ultrathin g-C_3N_4 surface towards superhigh photocatalytic and photoelectric performance. Appl Catal B-Environ, 2018, 237: 919–926
47 Wang X, Maeda K, Thomas A, *et al.* A metal-free polymeric photocatalyst for hydrogen production from water under visible light. Nat Mater, 2009, 8: 76–80
48 Xiang Q, Yu J, Jaroniec M. Preparation and enhanced visible-light photocatalytic H_2-production activity of graphene/C_3N_4 composites. J Phys Chem C, 2011, 115: 7355–7363
49 Liang Q, Li Z, Yu X, *et al.* Macroscopic 3D porous graphitic carbon nitride monolith for enhanced photocatalytic hydrogen evolution. Adv Mater, 2015, 27: 4634–4639
50 Ma TY, Dai S, Jaroniec M, *et al.* Graphitic carbon nitride nanosheet-carbon nanotube three-dimensional porous composites as high-performance oxygen evolution electrocatalysts. Angew Chem Int Ed, 2014, 53: 7281–7285
51 Yi SS, Yan JM, Wulan BR, *et al.* Noble-metal-free cobalt phosphide modified carbon nitride: An efficient photocatalyst for hydrogen generation. Appl Catal B-Environ, 2017, 200: 477–483
52 Lin Z, Wang X. Nanostructure engineering and doping of conjugated carbon nitride semiconductors for hydrogen photosynthesis. Angew Chem Int Ed, 2013, 52: 1735–1738
53 Feng Y, Yu XY, Paik U. Nickel cobalt phosphides quasi-hollow nanocubes as an efficient electrocatalyst for hydrogen evolution in alkaline solution. Chem Commun, 2016, 52: 1633–1636
54 Xin H, Guo K, Li D, *et al.* Production of high-grade diesel from palmitic acid over activated carbon-supported nickel phosphide catalysts. Appl Catal B-Environ, 2016, 187: 375–385
55 Huang Z, Chen Z, Chen Z, *et al.* Cobalt phosphide nanorods as an efficient electrocatalyst for the hydrogen evolution reaction. Nano Energy, 2014, 9: 373–382
56 Yang F, Chen Y, Cheng G, *et al.* Ultrathin nitrogen-doped carbon coated with CoP for efficient hydrogen evolution. ACS Catal, 2017, 7: 3824–3831
57 Zhang FS, Wang JW, Luo J, *et al.* Extraction of nickel from NiFe-LDH into Ni_2P@NiFe hydroxide as a bifunctional electrocatalyst for efficient overall water splitting. Chem Sci, 2018, 9: 1375–1384
58 Li Y, Zhang H, Jiang M, *et al.* Ternary NiCoP nanosheet arrays: An excellent bifunctional catalyst for alkaline overall water splitting. Nano Res, 2016, 9: 2251–2259
59 Ai G, Li H, Liu S, *et al.* Solar water splitting by TiO_2/CdS/Co-Pi nanowire array photoanode enhanced with Co-Pi as hole transfer relay and CdS as light absorber. Adv Funct Mater, 2015, 25: 5706–5713
60 Li X, Yu J, Low J, *et al.* Engineering heterogeneous semiconductors for solar water splitting. J Mater Chem A, 2015, 3: 2485–2534
61 Zhang LJ, Li S, Liu BK, *et al.* Highly efficient CdS/WO_3 photocatalysts: Z-scheme photocatalytic mechanism for their enhanced photocatalytic H_2 evolution under visible light. ACS Catal, 2014, 4: 3724–3729

Acknowledgements This work was supported by the National Natural Science Foundation of China (51702234) and the Natural Science Foundation of Tianjin City (18JCQNJC78800).

Author contributions Ma B fabricated the NiCoP/C_3N_4 nanohybrids and tested the photocatalytic activity; Zhao J fabricated the samples for control experiment; Ge Z did the characterization; Chen Y and Yuan Z designed the experiment and wrote the manuscript.

Conflict of interest The authors declare no conflict of interest.

Supplementary information A listing of supporting data (TGA curves of NiCoP-*x*/C_3N_4, Ni_2P-3/C_3N_4 and CoP-3/C_3N_4; XPS spectra of Ni 2p, Co 2p and P 2p of pristine NiCoP; SEM elemental mapping of C, N, Ni, Co and P for NiCoP-3/C_3N_4; TEM image of the bare g-C_3N_4; TEM image of NiCoP-3/C_3N_4 and NiCoP particle size distribution on g-C_3N_4; EDX spectrum of the as-prepared NiCoP-3/C_3N_4 in TEM; digital photo of the NiCoP, g-C_3N_4 and NiCoP-*x*/C_3N_4; UPS of g-C_3N_4 and NiCoP-3/C_3N_4; comparison of photocatalytic H_2 production rate of NiCoP-3/C_3N_4 and Pt-3/C_3N_4 under UV-Vis light; cycling tests of NiCoP-3/C_3N_4 for H_2 evolution; PL spectra of g-C_3N_4, Ni_2P-3/C_3N_4, CoP-3/C_3N_4 and NiCoP-3/C_3N_4; EIS results of Ni_2P-3/C_3N_4, CoP-3/C_3N_4 and NiCoP-3/C_3N_4; comparison of the photocatalytic hydrogen production performance of NiCoP/g-C_3N_4 with the literatures) are available in the online version of the paper.

Bo Ma received his Bachelor's degree in 2009, Master's degree in 2013 and PhD in 2017 from Nankai University. His research interest focuses on the carbon-based non-noble metal materials for photocatalysis and electrocatalysis.

Yantao Chen received his BSc degree in 2009 from the University of Science and Technology of China and his PhD degree in 2014 from Brown University, USA. In 2015, he worked as a postdoctoral associate at the University of Wisconsin-Milwaukee. In 2016, he joined Tianjin University of Technology as a full professor. His research interest lies in functional nanomaterials for electrochemical applications.

Zhihao Yuan obtained his PhD from the Institute of Solid State Physics, CAS, in 1996. Following post-doctoral experience in Tsinghua University, he joined Tianjin University of Technology as a full professor in 2002. His main research interest includes photoelectric nanomaterials and devices, nano-catalysis and nano-photocatalysis, and semiconductor-based gas sensor.

负载5 nm磷化钴镍纳米颗粒的石墨相氮化碳高效光催化产氢催化剂

马博, 赵金苹, 葛振华, 陈衍涛*, 袁志好*

摘要 本文通过可控醇热反应将5 nm磷化钴镍纳米颗粒负载在石墨相氮化碳上得到一种高效催化产氢催化剂. 磷化钴镍是优良的电子导体和光催化反应助催化剂. 通过原位生长法将微小的磷化钴镍纳米颗粒和氮化碳复合可有效消除磷化钴镍的光遮蔽效应, 同时抑制光生载流子的复合, 提高载流子的迁移率. 由此, 磷化钴镍/氮化碳纳米复合物表现出远高于纯氮化碳, 单独的磷化镍或磷化钴/氮化碳复合物的光催化产氢活性. 本研究为构筑过渡金属磷化物基光催化剂提供了崭新的思路.

 © Science China Press and Springer-Verlag GmbH Germany, part of Springer Nature 2019